



ELSEVIER

Contents lists available at ScienceDirect

European Polymer Journal

journal homepage: www.elsevier.com/locate/europolj

Thermo-rheological behaviour of native silk feedstocks

Peter R. Laity, Chris Holland

Department of Materials Science and Engineering, The University of Sheffield, Sir Robert Hadfield Building, Mappin Street, Sheffield S1 3JD, UK

ARTICLE INFO

Article history:

Received 26 July 2016

Received in revised form 19 October 2016

Accepted 31 October 2016

Available online xxxxx

Keywords:

Silk feedstock

Rheology

Temperature dependence

Activation energy

ABSTRACT

The rheology of native silk protein feedstock specimens was characterised by shear and oscillatory measurements, over the temperature range from 2 to 55 °C, producing no evidence of thermally-driven phase change behaviour. All specimens exhibited flow characteristics typical of a concentrated polymer solution, with visco-elastic behaviour dominated by two main relaxation modes exhibiting time constants around 0.44 and 0.055 s at 25 °C. The specimens showed well-behaved temperature dependence following the Arrhenius equation, consistent with the kinetics being governed by an activation energy of flow, which ranged from 30.9 to 55.4 kJ mol⁻¹ based on oscillatory data. Consequently, for the first time, it was possible to compile master-curves for native silk feedstock specimens following the principles of time-temperature superposition, using oscillatory data demonstrating visco-elastic behaviour typical of a polymer solution across a wide temperature range. Our work has highlighted the processing range of natural silks and furthered our stance on the molecular mechanisms governing the flow behaviour of these interesting and important materials.

© 2016 The Authors. Published by Elsevier Ltd. This is an open access article under the CC BY license (<http://creativecommons.org/licenses/by/4.0/>).

1. Introduction

The ability to spin silk fibres is a remarkable feature of many types of arthropods [1], exhibited by numerous species of insects [2–4], notably Lepidoptera larvae (*i.e.* caterpillars) [4–8], and is a defining characteristic of spiders [9,10]. In spite of the diversity of animals with this ability, however, in all cases, the fibres are produced in a similar way, from protein feedstock that is synthesised and stored in special glands inside the body, then spun, solidifying ‘on demand’ [11–14].

As would be expected for a biological process, natural silk spinning uses an aqueous medium at body temperatures (*i.e.* essentially ambient temperatures for ectothermic animals). This is in stark contrast to industrial fibre spinning, which typically involves esoteric or harmful process chemicals (for wet- or dry spinning) or high temperatures (for melt spinning) [15,16], in order to engineer sufficiently large changes in physical conditions or chemical composition to drive solidification and stabilise the nascent fibres.

Clearly, the conversion mechanism from liquid feedstock to solid fibre under such mild conditions must play a key role in natural silk spinning. This appears to occur by a flow-induced phase change, as the silk feedstock passes through the spinning duct or is drawn into a fibre, on leaving the body [10–14,17–27]. Notwithstanding numerous investigations, however, some of the structural mechanisms for this proposed phase change can appear contradictory or counter-intuitive, thus leaving the precise details somewhat conjectural. In particular, several authors have based their explanations on the proteins (*i.e.* fibroin or spidroin) adopting folded structures in the silk feedstock, which are unfolded by flow stress, promoting coagulation through hydrophobic interactions [23] or ionic crosslinks [25,26], followed by hydrogen bonding and culminating in β -

E-mail addresses: petelaity@aol.com (P.R. Laity), christopher.holland@sheffield.ac.uk (C. Holland)

<http://dx.doi.org/10.1016/j.eurpolymj.2016.10.054>

0014-3057/© 2016 The Authors. Published by Elsevier Ltd.

This is an open access article under the CC BY license (<http://creativecommons.org/licenses/by/4.0/>).

sheet formation. Yet the idea of silk proteins having folded tertiary structures akin to those seen in other *in vivo* globular proteins appears to be contradicted by experimental evidence from Raman spectroscopy [24], circular dichroism (CD) studies [28–32], small-angle neutron scattering (SANS) [32] and nuclear magnetic resonance (NMR) spectroscopy [33–36]. Hence, as we have argued previously [37], the fibroin in native silk feedstock appears more similar to the recently defined class of intrinsically disordered proteins (IDP) [38,39], rather than a precisely-folded globular protein. This forms the basis for our investigations into the rheology and phase change behaviour of native silk feedstocks.

It is generally accepted that the rheology of the native silk feedstock is an important factor in the spinning process, which has led to numerous publications [37,40–51]. Recent detailed investigations from our group into the rheology of native silk feedstocks from the domesticated mulberry silk moth (*Bombyx mori*) larvae at 25 °C [37,40] confirmed it is a viscoelastic material with properties typical of a polymer solution. These studies also highlighted considerable natural variability of rheological properties, however, notwithstanding the consistent methods used to obtain the specimens [40]. Even more remarkably, in spite of this rheological variability, it was found that normalising with respect to the cross-over modulus (G_x) and angular frequency (ω_x) consistently reduced the oscillatory data onto master-curves of $\log(G'/G_x)$ and $\log(G''/G_x)$ against $\log(\omega/\omega_x)$ [37]. For the first time this demonstrated a 'rheological simplicity' between the data and excluded potential explanations such as incipient gelation, which would have changed the shape of the master-curves.

To date, the majority of native silk rheology studies have yet to investigate the effect of temperature on the feedstock; those that have tended to focus on irreversible gelation effects brought about by raising temperature [43,47,50]. On the contrary, we believe focussing on changes in silk flow behaviour *below* the gelation temperature provides new perspectives onto the silk spinning process and is the subject of our present work.

Natural silk spinning can be observed over a relatively wide temperature range and, since all known producers are ectothermic, it follows that the environmental and feedstock temperatures during spinning are largely identical. For example, caterpillars of the arctic moth *Gynaephora groenlandica* spin silk cocoons and hibernacula at typical daytime (maximum) temperatures of 5–10 °C [52], while tropical species of silkworms [53] or spiders [54–56] may experience ambient temperatures above 35–40 °C. Clearly, compositional differences between the silk feedstocks of these species may facilitate spinning under these different conditions. Nevertheless, fibre spinning over significant temperature ranges has also been reported for single species in captivity (e.g. 5–30 °C for *Achaearanea tepidariorum* [57]; 5–42 °C for *Araneus diadematus* spiders [58,59]; 22–38 °C for the silkworm *B. mori* [60]).

From a polymer science standpoint, changes in the flow behaviour of 'well-behaved' polymer systems at different temperatures generally follow the time-temperature superposition (TTS) principle [61–64]. Using the TTS principle, phase changes or other factors affecting the flow behaviour may be revealed in the temperature dependence (required to superimpose results onto a single master curve). Hence, for example, Liao and co-workers analysed the effects of monomer ratio in poly(hydroxybutyrate-co-hydroxyhexanoate) copolymers [65]; Osterwinter et al. observed the effects of hydrogen bonding in partially and permethylated polyglycerols [66] and Rwei and Lyu were able to locate the onset of liquid crystalline behaviour in a cellulosic system [67].

Thus, our present work seeks to examine in detail how the rheology of the liquid feedstock of *B. mori* changes with temperature. As silk flow behaviour is apparently governed by classical polymer rheology relationships [37,40], one might also expect to find that it exhibits TTS. Firstly, this will contribute to understanding how the ambient conditions may affect silk spinning. Secondly, studying changes in flow behaviour with temperature may help to explain the rheological variability observed for native silk feedstocks and the thermodynamic mechanisms behind its flow-induced phase change.

2. Experimental

Native silk feedstock specimens were obtained from 5th instar *B. mori* larvae (commercially bred four-way poly-hybrid cross of 2 Japanese and 2 Chinese strains) during early stages of cocoon construction and characterised using methods similar to those described previously [37,40]. In summary, silk glands were excised and the epithelial membrane was peeled off under cold (ca. 5 °C) distilled water, using fine tweezers and a dissection microscope. A portion (ca. 0.01–0.02 g) of the (predominantly) fibroin solution from the middle posterior section of the gland was carefully and promptly (within 30 s) transferred to a rheometer (Bohlin Gemini, Malvern Instruments Ltd. Malvern, UK), fitted with a Peltier heating and cooling stage and a CP1/10 geometry (10 mm diam. cone with 1° opening angle and 30 μm truncation). Excess water was removed from the surface of the specimen, by absorbing it into a small piece of tissue paper, before lowering the cone. The closing speed was reduced to the slowest (ca. 0.1 mm s⁻¹), to minimise the associated (shear and extensional) flow. The sample size was sufficient to completely fill the gap between the cone and plate; the loading was carefully observed by eye and any inadvertently under filled or unevenly filled samples were rejected. The small amount of excess material around the cone was not removed, to avoid any risk of flow-induced gelation. The entire sample area was flooded with distilled water, then enclosed within a loosely fitting cover to prevent drying and skin formation.

At the same time, a larger portion (0.1–0.2 g) of the native silk feedstock from the adjacent part of the gland was also removed and used to determine the concentration of solid residue (mainly fibroin [40]). In order to minimise possible weighing errors due to water evaporation, this specimen was weighed at the same time as the rheology specimen was loaded. (Hence, with practice, the weighing was generally performed within 1 min. after removing the gland epithelium.) After

drying to constant weight under vacuum at 60 °C, a protein concentration in the range 19–30% w/w was obtained, in good agreement with previous results [40].

The rheometer was controlled using the Bohlin software, which also performed the initial data processing. Rheological behaviour of each specimen was determined using sequences of shear and oscillatory measurements, which were run as 'job-streams' within the Bohlin software. Each experiment began at 25 °C, with a period of constant shear rate (100 s at $\dot{\gamma} = 1 \text{ s}^{-1}$), in order to supersede any residual stress due to loading and to distribute the specimen evenly between the cone and plate. The apparent viscosity at this shear rate (η_1) was evaluated by averaging the data over the final 30 s. The relaxation behaviour was also characterised at 25 °C, from a series of oscillatory measurements (25–0.1 Hz, equivalent to angular frequencies of $\omega = 157\text{--}0.63 \text{ rad s}^{-1}$). Then, in the majority of experiments, changes in relaxation behaviour with temperature (T) were characterised by further oscillatory measurements between 2 and 55 °C. In order to check for irreversible changes during the course of the experiments, the final oscillatory measurements were performed after returning to 25 °C.

As a control, experiments were also performed to check the stability of the native silk feedstock. In these cases, repeated oscillatory measurements were performed on specimens held at constant temperature for extended periods (11 sweeps over approximately one hour, at 25 °C or 55 °C).

As reported previously [37,40], both the elastic and viscous moduli could be fitted well using binary expressions based on the Maxwell model [62–64,68–71]:

$$G'(\omega) = g_1 \left(\frac{\omega^2 \tau_1^2}{1 + \omega^2 \tau_1^2} \right) + g_2 \left(\frac{\omega^2 \tau_2^2}{1 + \omega^2 \tau_2^2} \right) \quad (1a)$$

$$G''(\omega) = g_1 \left(\frac{\omega \tau_1}{1 + \omega^2 \tau_1^2} \right) + g_2 \left(\frac{\omega \tau_2}{1 + \omega^2 \tau_2^2} \right) \quad (1b)$$

where g_i combines the modulus term and the weighting (i.e. $g_i = p_i G_i$). Hence, g_i and τ_i for the two main relaxation modes were evaluated by simultaneously fitting these equations to the G' and G'' data, using the 'Solver' routine in Excel® (Microsoft® Office) software.

3. Results

3.1. Changes in rheology with time

Prior to investigating the changes in rheology at different temperatures, it was necessary to check the stability of the native silk feedstock over timescales commensurate with these experiments. This is demonstrated by the results shown in Fig. 1.

Control experiments were performed at constant temperature for extended periods (11 frequency sweeps over approximately 55 to 62 min, at 25 °C or 55 °C). Since it is known that native silk feedstock specimens can show considerably variable properties [37,40], results are compared from specimens with reasonably similar viscosities (1468 and 2217 Pa s at $\dot{\gamma} = 1 \text{ s}^{-1}$). Values of $\log(G')$ and $\log(G'')$ from the initial and final sweeps are plotted against $\log(\omega)$ in Fig. 1a and b, (at 25 and 55 °C respectively). At both temperatures, these data showed classic viscoelastic behaviour: the elastic modulus dominated at higher frequency, with a cross-over to viscous behaviour at lower frequency. This is typical of a polymer solution, where the rheology is dominated by the behaviour of the high molecular weight solute [62–64,68–71]. By direct comparison of these data, it was found that the plots of $\log(G')$ and $\log(G'')$ became steeper towards low frequencies and the cross-over frequency (ω_x) increased (from 5.9 to 23.9 rad s^{-1}) at the higher temperature, consistent with the specimens becoming more fluid.

In each case, small decreases in the dynamic moduli at fixed frequencies were observed over the course of the experiments. This was probably due to the gradual dilution or partial dissolution of the specimens by the water used to prevent drying out and skin formation (which were considered to pose a greater problem), as we shall explore briefly, below.

The binary model described by Eq. (1) appeared to fit the oscillatory data quite well, as demonstrated in Fig. 1a and b. This was consistent with recent findings [37,40], which suggested that the rheology of the native silk feedstocks was dominated by two main relaxation modes with characteristic time constants (τ_i) around 0.44 and 0.055 s. In keeping with the designations used previously, these are referred to as modes 3 and 4, respectively. It may be noted that small contributions from two slower processes (with time constants around 66 and 3.5 s, designated modes 1 and 2) have been observed by stress relaxation measurements [40]; their role in silk rheology is discussed further in a separate paper [72].

Hence, by fitting the model to the data, it was possible to evaluate the viscoelastic parameters (g_i and τ_i) describing these dominant relaxation modes 3 and 4; the results are shown in Fig. 1c–f. Over the course of the control experiment held at 25 °C, the modulus contributions for both modes 3 and 4 (in Fig. 1c) appeared to decrease slightly, although these changes were barely significant in view of the uncertainty expected. Somewhat larger changes were observed for the control experiment held at 55 °C (in Fig. 1d), with decreases of around 20% for g_4 and closer to 50% for g_3 . These changes in g_i would be consistent with the samples being slowly diluted or material being dissolved during the course of the experiments, as noted above.

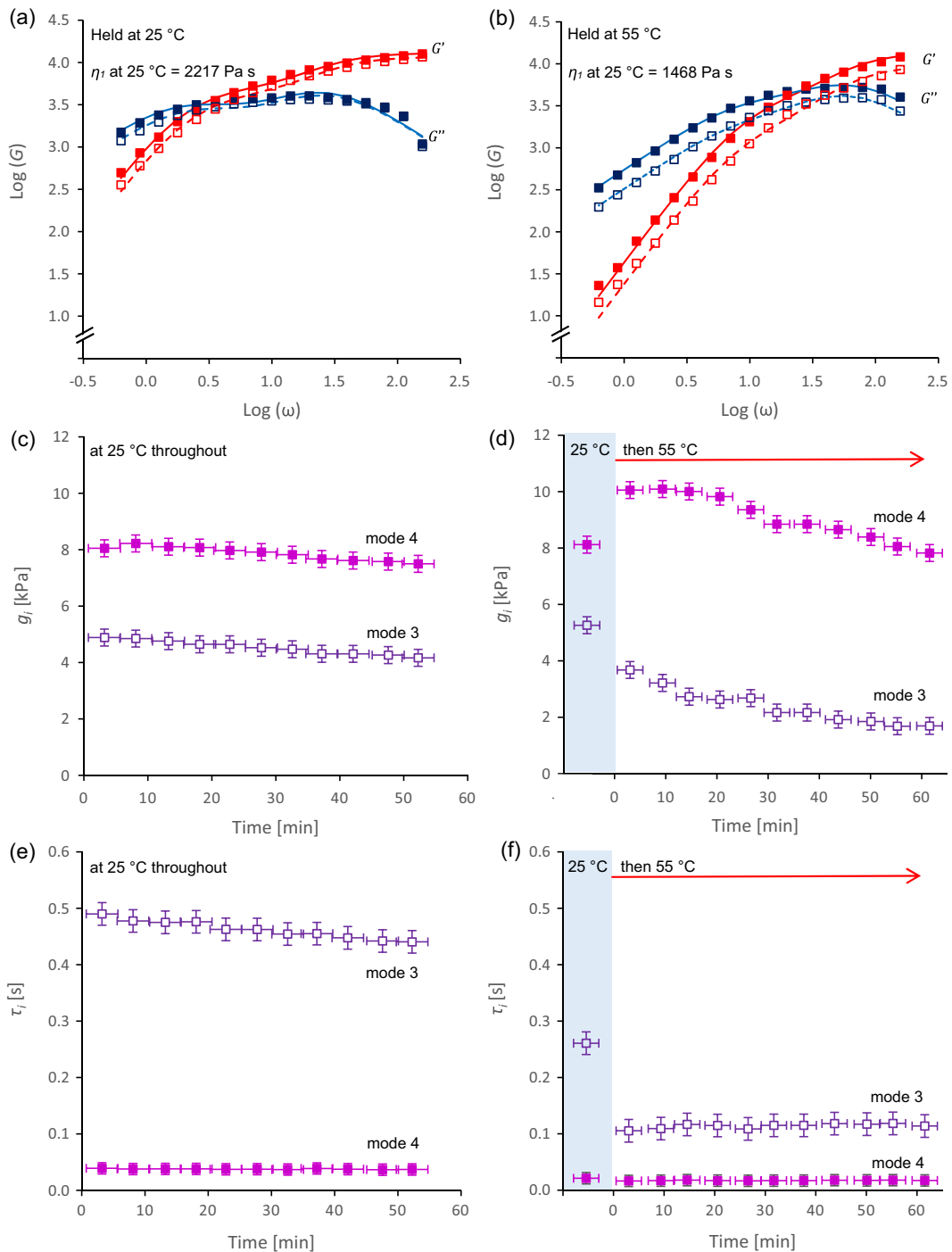


Fig. 1. Oscillatory data to check the stability of native silk feedstock specimens under the experimental conditions: (a and b) plots of $\log(G)$ against $\log(\omega)$, from the initial and final frequency sweeps (filled and open symbols) and corresponding model fits using the binary Maxwell model (Eq. (1), solid and dashed lines), for specimens held at 25 °C or 55 °C; (c–f) changes with time during experiments at constant temperatures, for the viscoelastic parameters describing the two faster modes, obtained from repeated oscillatory sweeps at 25 and 55 °C: (c and d) modulus contributions; (e and f) relaxation rate constants extracted from data by fitting Eq. (1). The horizontal error bars correspond to the time required to perform an oscillatory sweep (≈ 5 min), while the vertical error bars indicate the expected uncertainty in the results. The points in the shaded areas (in d and f) correspond to results from the initial measurements at 25 °C, for specimens subsequently held at 55 °C. Note: the longer relaxation times (in e and f) corresponded to the smaller modulus contributions (in c and d).

Rather interestingly, the relaxation time constants at 25 and 55 °C (in Fig. 1e and f) exhibited considerably less change compared with the modulus contributions. In particular, τ_4 remained effectively constant during the periods at either temperature, while τ_3 appeared to decrease slightly (by ca. 8%) at 25 °C but to increase by a similar amount at 55 °C. It is expected that the relaxation time constants would be dominated by the molecular scale environment, through the distances between neighbouring chain segments (*i.e.* concentration affecting the reptation tube diameter) and intermolecular forces [62–64,68–71]. By contrast, the modulus contributions could also be affected by changes in the quantity of material. Hence, the differences in behaviour between the relaxation time constants and modulus contributions suggest that dissolution of excess material from around the cone, rather than dilution of the specimen under the cone, was probably the main factor effecting the changes observed in these experiments at constant temperature.

The rates of change observed over the extended timescales of these experiments were considered to be acceptably small, in view of the shorter times required to perform the oscillatory measurements at different temperatures. Hence, this established a framework against which the larger changes due to temperature could be judged.

Most importantly, these results showed no evidence of thermal gelation over the timescales of the experiments at 55 °C – even though this was 17 °C above the critical (*i.e.* onset) temperature reported by Moriya *et al.* [47] for native silk feedstocks from *B. mori*. It appears, therefore, that the thermal gelation process may not be quite as consistent as suggested by that work. Sample-to-sample variability in the critical temperature and subsequent rate of phase change may offer an explanation. Alternatively, we note that those authors used a solvent trap and regulator to prevent the specimens drying out, whereas we have found such systems to be unreliable for experiments performed over longer timescales or higher temperatures.

3.2. Changes in rheology with temperature

Some evidence of temperature dependence in the rheology of native silk feedstocks from *B. mori* is shown by the results shown in Fig. 1. More comprehensive data from experiments on representative specimens are presented in Fig. 2.

Changing temperature produced significant responses in the elastic and viscous moduli, as shown in Fig. 2a. These were most pronounced for the elastic modulus towards lower frequencies, causing the cross-over frequency to rise, corresponding to increased fluid-like behaviour. It should be noted that these changes due to temperature appeared qualitatively different from those observed over time at constant temperature in the control experiments (Fig. 1a and b), which resulted in roughly parallel downward shifts of both the G' and G'' curves.

The increase in fluidity at higher temperatures is also demonstrated in Fig. 2b. A smooth decrease was observed for the modulus of complex viscosity ($|\eta^*|$), extracted directly from the oscillatory data at the lowest frequency, $\omega = 0.63 \text{ rad s}^{-1}$) or the zero-shear viscosity, which was estimated using:

$$\eta_0 \approx g_3\tau_3 + g_4\tau_4 \quad (2)$$

It was shown previously [40] that using this equation with values of τ_i and g_i obtained by fitting the binary Maxwell model (Eq. (1)) to oscillatory data produced good agreement with the values of η_1 measured directly. Moreover, in the present work, close agreement was observed between the values of $|\eta^*|$ at 0.67 rad s^{-1} and calculated values of η_0 , suggesting that these parameters may effectively be used interchangeably. These viscosities decreased smoothly with increasing temperature and appeared to follow an approximately exponential curve, with the values at 10 °C around 3.5 times higher than those at 40 °C. The cross-over frequency increased smoothly with temperature, also following an approximately exponential relationship, the value at 40 °C being about 4.7 times higher than at 10 °C.

Changes in the values of τ_i and g_i with temperature are shown in Fig. 2c and d. In order to increase the number of points without having to run excessively long experiments, data was aggregated from four specimens with similar shear viscosity ($\eta_1 = 1757\text{--}2242 \text{ Pa s}$ at 25 °C).

A logarithmic vertical axis is used to accommodate the wide range of relaxation time constants (in Fig. 2c), which spanned almost two orders of magnitude from (the slower) mode 3 at 2 °C to (the faster) mode 4 at 55 °C. The τ_i values for both modes decreased smoothly with increasing temperature, consistent with the expectation of faster relaxation rates as the specimens became more fluid. Larger changes were observed for mode 3 than mode 4, however; the former decreased by around 60% (from 0.559 to 0.229 s) between 10 and 40 °C, while the latter decreased by around 30% (from 0.0303 to 0.0212 s) over the same temperature range.

The corresponding plots of g_i (in Fig. 2d) for mode 3 and 4 followed opposite trends, with the former decreasing, while the latter became more dominant at higher temperature. Based on the concept of 'entropic springs' [62–64,68–71], it would be expected that the modulus should increase with temperature. The analysis performed here generated values of modulus contributions, however, which also depended on the number of conceptual spring elements involved. Hence, these results might suggest some form of temperature-dependent interconversion between the mode 3 and mode 4 processes.

It should also be noted that these changes due to temperature appeared to be reversible; hence, similar results were obtained from the initial and final measurements at 25 °C. This was demonstrated most clearly by the viscosities and cross-over frequencies (in Fig. 2b), but was also evident in the extracted values of τ_i and g_i (in Fig. 2c and d). Again, this argues against thermally-induced phase change occurring within the experimental timescale and temperature range explored.

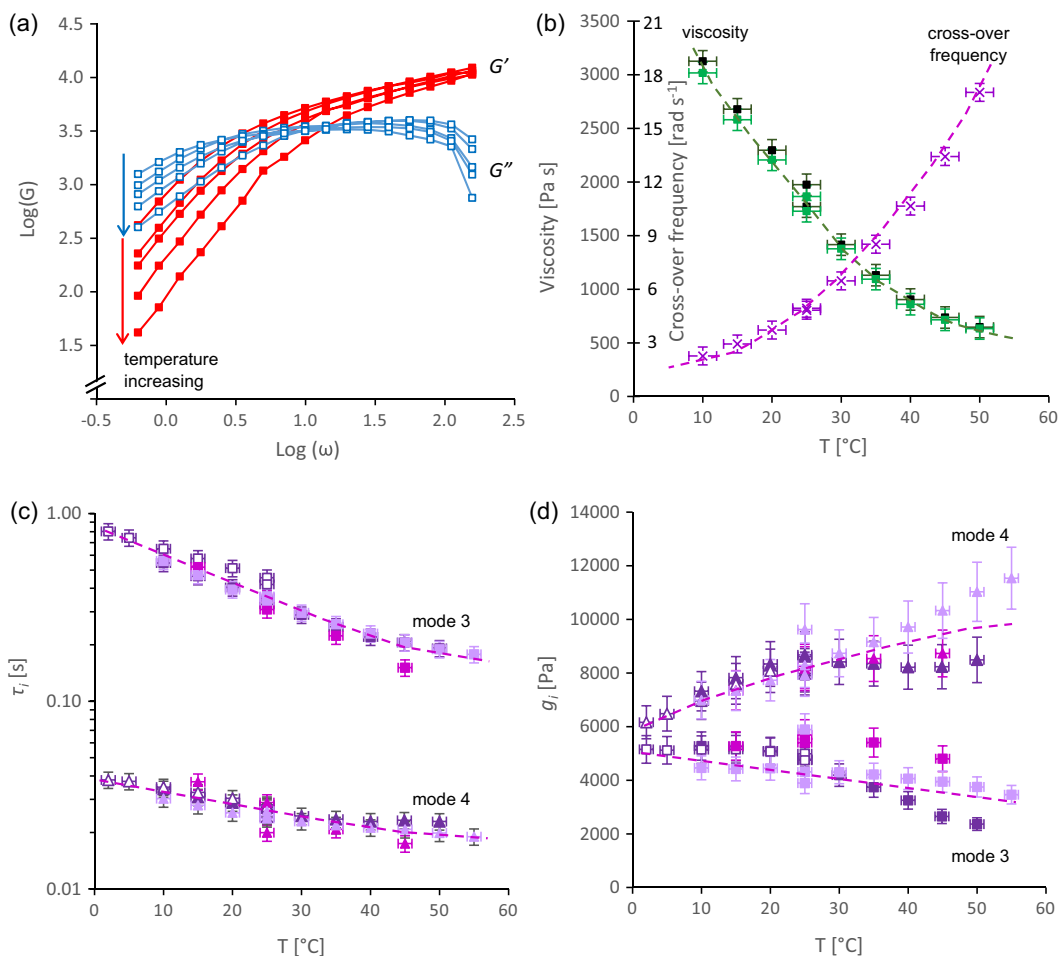


Fig. 2. Rheological data measured at different temperatures, for typical specimens of native silk feedstock: (a) oscillatory sweeps; (b) complex viscosity at 0.63 rad s^{-1} (filled symbols), zero-shear rate viscosity calculated from oscillatory data using Eq. (2) (open symbols) and angular frequency at the cross-over, for a typical specimen of native silk feedstock. Changes with temperature, for: (c) relaxation times and (d) modulus contributions for modes 3 and 4, obtained by model fitting using Eq. (1), for four similar specimens of native silk feedstock. The horizontal error bars in b, c and d correspond to the largest uncertainty expected in the temperature ($\pm 1 \text{ }^\circ\text{C}$), while the vertical error bars indicate the expected uncertainty in the results. The different symbols represent different specimens. The dashed lines in b, c and d merely provide a guide for the eye.

A clearer picture of the effects of temperature on flow behaviour is presented in Fig. 3. Again, aggregated results from four experiments on similar specimens are shown, corresponding to the data in Fig. 2. It appeared that the changes in viscosity, cross-over frequency and relaxation times all followed Arrhenius-type relationships, as described by:

$$X(T) = X_0 \exp\left(\frac{kE_a}{RT}\right) \quad (3)$$

where $k = -1$ for a rate (e.g. relaxation frequency) or $+1$ for an inverse rate (such as viscosity or relaxation time constants), the pre-exponential factor X_0 is a constant describing the property under reference conditions and R is the gas constant. Hence, for each of these parameters, plotting $\log(X)$ vs. $1/T$ gave a straight line with slope proportional to E_a .

E_a is usually interpreted as the activation energy for the rheological process, representing the magnitude of (energy) barriers impeding segmental rotations and changes in chain configuration. In reality, though, it reflects a more general temperature dependence, which may be expected to incorporate additional factors, such as thermally driven changes in solvent quality. Consequently, it may be more appropriate to use the expression ‘apparent activation energy’.

Notwithstanding these reservations, the slopes of the graphs in Fig. 3 yielded the following values for the apparent activation energy:

- 31.8 kJ mol^{-1} from the calculated zero-shear viscosity or modulus of complex viscosity;
- 42.2 kJ mol^{-1} from the cross-over frequency;
- 23.6 kJ mol^{-1} from mode 3 relaxation time;
- 9.9 kJ mol^{-1} from mode 4 relaxation time.

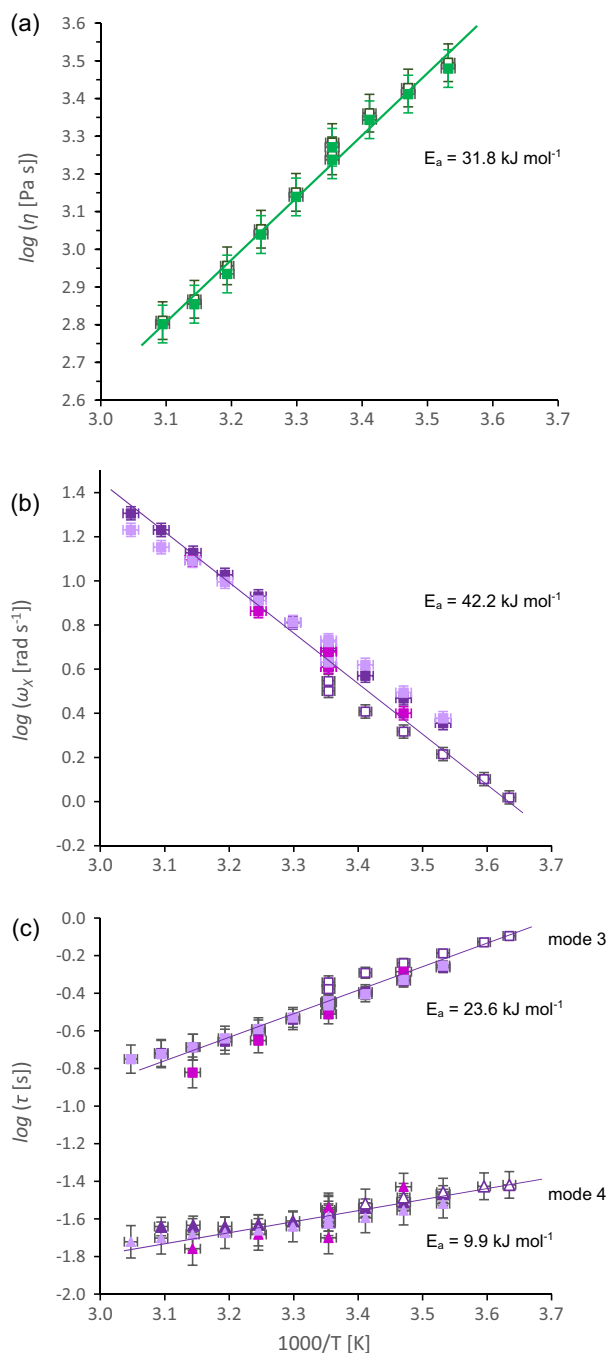


Fig. 3. Arrhenius plots of (a) $\log(\eta)$, (b) $\log(\omega\chi)$, (c) $\log(\tau_i)$ for modes 3 and 4 vs. $1000/T$. The results correspond to the data shown in Fig. 2; different symbols represent different specimens. The resulting values of activation energy are shown in each graph.

Different values of E_a may be expected from different molecular processes. Moreover, even though simple relationships may exist between some parameters, more complex relationships between the corresponding values of E_a may ensue. This can be demonstrated by considering the zero-shear viscosity and relaxation times, which are related through Eq. (2). Hence, using the chain rule for differentiation:

$$\frac{d}{d(1/T)} \log(\eta_0) = \frac{d}{d(1/T)} \log(g_3\tau_3 + g_4\tau_4) \quad (4a)$$

$$= \frac{d}{d(g_3\tau_3 + g_4\tau_4)} \log(g_3\tau_3 + g_4\tau_4) \cdot \frac{d}{d(1/T)} (g_3\tau_3 + g_4\tau_4) \quad (4b)$$

$$= \frac{1}{(g_3\tau_3 + g_4\tau_4)} \cdot \frac{d}{d(1/T)} (g_3\tau_3 + g_4\tau_4) \quad (4c)$$

The results presented in Fig. 2 show that all four parameters (τ_3 , τ_4 , g_3 and g_4) varied with T (and, hence $1/T$). Consequently, the full derivative is:

$$\frac{d}{d(1/T)} \log(\eta_0) = \frac{1}{\eta_0} \cdot \left(g_3 \frac{d}{d(1/T)} \tau_3 + \tau_3 \frac{d}{d(1/T)} g_3 + g_4 \frac{d}{d(1/T)} \tau_4 + \tau_4 \frac{d}{d(1/T)} g_4 \right) \quad (4d)$$

which clearly demonstrates that no simple relationship should be expected between the activation energies obtained from these different parameters.

On the other hand, a strong inverse correlation between viscosity and cross-over frequency has been reported previously [37]. It was found that ω_X decreased as η_1 increased, closely following an inverse power-law relationship described by:

$$\omega_X = 1427\eta_1^{-0.767} \quad (5a)$$

$$\ln(\omega_X) = \ln(1427) - 0.767 \ln(\eta_1) \quad (5b)$$

This relationship reflected the fact that the relaxation times became longer for the more viscous specimens, although an explanation for the precise fractional value of the power-law exponent cannot be given at present. Moreover, as ω_X was obtained from oscillatory measurements while η_1 was measured in constant shear, the strength of this correlation imparts confidence in both sets of measurements.

Consequently, a simple relationship also emerged between the values of E_a obtained from ω_X and $|\eta^*|$, as demonstrated in Fig. 4. The Arrhenius expressions for these parameters are:

$$\ln(|\eta_1|) = \ln A_\eta + \frac{E_\eta}{RT} \quad (6a)$$

$$\ln(\omega_X) = \ln A_\omega - \frac{E_\omega}{RT} \quad (6b)$$

where the subscripts indicate the parameter being measured. Substitution into Eq. (5b) gives:

$$\ln A_\omega - \frac{E_\omega}{RT} = \ln 1427 - 0.767 \left\{ \ln A_\eta + \frac{E_\eta}{RT} \right\} \quad (6c)$$

After collecting the various constants together as C , this equation can be simplified to give:

$$E_\omega = CT + 0.767E_\eta \quad (6d)$$

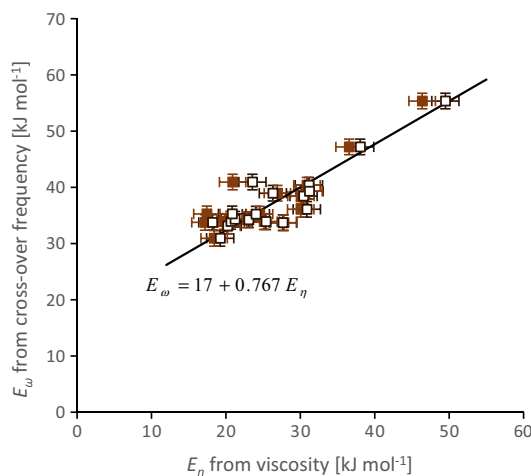


Fig. 4. Relationship between values of apparent activation energy derived from complex viscosity at 0.63 rad s^{-1} (filled symbols) or zero-shear rate viscosity calculated from oscillatory data using Eq. (2) (open symbols) and cross-over frequency. The error bars were obtained by manually fitting plausible trend lines with the greatest and least slopes through the Arrhenius plots (as in Fig. 3). The line represent the relationship described by Eq. (6d).

This appeared to fit the relationship between these results quite well, as demonstrated in Fig. 4. Over the range investigated, E_{ω} was consistently larger but increased more slowly than E_{η} . Moreover, these values of E_{ω} were derived from different parameters and may seem to be independent whereas, in fact, they were correlated.

This raises the question as to which parameters should be used to extract the most meaningful values of activation energies. One might expect that the relaxation times for the two dominant modes (τ_3 , τ_4) would be likely candidates; however, as already noted, the behaviour shown by the modulus contributions (g_3 and g_4) in Fig. 2d may be consistent with interconversions between these oscillatory processes. Hence, the variations in relaxation times with temperature may reflect qualitative changes in the underlying molecular processes, in addition to quantitative changes in their rates. Instead, for the present, attention is directed towards the viscosity and cross-over frequency, which have the advantage of being easily recognised, macroscopic phenomena. As already demonstrated, however, they are not independent. Moreover, the importance of ω_X in analysing oscillatory the data has already been demonstrated: normalisation with respect to the cross-over frequency and modulus reduced the oscillatory data from specimens with widely differing shear viscosities onto a master-curve [37]. Conversely, however, viscosity and the cross-over frequency may be somewhat removed from the underlying molecular-scale mechanisms and may depend on combinations of these processes.

The temperature dependences shown by the modulus of complex viscosity ($|\eta^*|$ at $\omega = 0.63 \text{ rad s}^{-1}$) and cross-over frequency are demonstrated in the form of Arrhenius plots, in Fig. 5a and b, for selected specimens with a wide range of shear viscosities ($\eta_1 = 417\text{--}1999 \text{ Pa s}$ at $25 \text{ }^\circ\text{C}$). In each case, irrespective of η_1 , the data followed a straight line, consistent with the rate being controlled by an activation energy. The inverse relationship between ω_X and η_1 at $25 \text{ }^\circ\text{C}$ that was demonstrated in Fig. 2 was also evident here: hence, plots for the more viscous specimens lay below those of the more fluid samples in Fig. 5b (based on ω_X).

Apparent activation energy values derived from viscosity data ranged from 17.2 to 49.5 kJ mol^{-1} , for specimens with η_1 values from 208 to 4686 Pa s . Close agreement was observed between the results based on $|\eta^*|$ and η_0 , consistent with the effective equivalence of these parameters, as demonstrated previously (in Fig. 2b). The E_{η} values are plotted against the shear viscosity at $25 \text{ }^\circ\text{C}$ in Fig. 5c. Notwithstanding a certain amount of variability, these results appeared to follow a weak negative correlation, decreasing as the viscosity increased. The best (albeit limited, $R^2 = 0.44$) correlation was achieved with a logarithmic model, which was described by:

$$E_{\eta} = 141\eta_1^{-0.24} \quad (7)$$

The range of E_{η} values obtained suggested considerable compositional differences between the native silk protein specimens used, which may be linked to the proteins present or the solvent composition. Indeed, variations in protein concentration (from 19.4 to 29.2% , in line with previous measurements [40]) were found amongst the full set of specimens used to compile Fig. 5c; however, restricting the data to specimens within a narrower concentration range (from 21 to 23%) did not significantly reduce the range of E_{η} values observed or improve the correlation.

Arguably, this might still leave room for uncertainty. In addition to possible changes in protein concentration during sample preparation and over the course of an experiment, systematic variations along the silk gland (from *ca.* 12% in the posterior section to 26% in the middle section) have been reported [50]. Hence, this could lead to discrepancies between the concentration determined gravimetrically and that in the adjacent portion used for rheology. This potential error seems negligible, however, since similar results were obtained irrespective of whether the rheology specimens were taken ‘up-stream’ or ‘down-stream’ of the adjacent gravimetric samples.

The corresponding set of apparent activation energy values derived from the cross-over frequency is shown in Fig. 5d. This graph showed a resemblance to Fig. 5c, but was displaced to higher values of apparent activation energy ($30.9\text{--}55.4 \text{ kJ mol}^{-1}$) – particularly towards the higher viscosities. As already noted, a relationship was derived between E_{ω} and E_{η} , as described by Eq. (6d). Hence, substituting Eq. (7) into Eq. (6d) yields:

$$E_{\omega} = CT + 0.767(141\eta_1^{-0.24}) \quad (8a)$$

$$= CT + 108 \cdot \eta_1^{-0.24} \quad (8b)$$

which should describe the relationship between E_{ω} and η_1 . This did not provide a particularly good description of the data, however, probably as a consequence of compounding the relatively poor correlations already present with Eqs. (6d) and (7). Consequently, it was not possible to describe any systematic trend between E_{ω} and η .

3.3. Time-temperature superposition of oscillatory plots

It was found that oscillatory data collected at different temperatures could be made to converge onto a ‘master-curve’, following suitable scaling in the horizontal and vertical directions. This is demonstrated in Fig. 6, for a typical native silk feedstock specimen (with $\eta_1 = 1757 \text{ Pa s}$ at $25 \text{ }^\circ\text{C}$). Individual measurements between 10 and $55 \text{ }^\circ\text{C}$ are shown in Fig. 6a, while the results after TTS are shown in Fig. 6b.

The scaling parameters for the TTS describe how the flow behaviour changes with temperature, relative to that at a reference temperature (T_0) [62–64,68–71]. For the frequency (horizontal) axis:

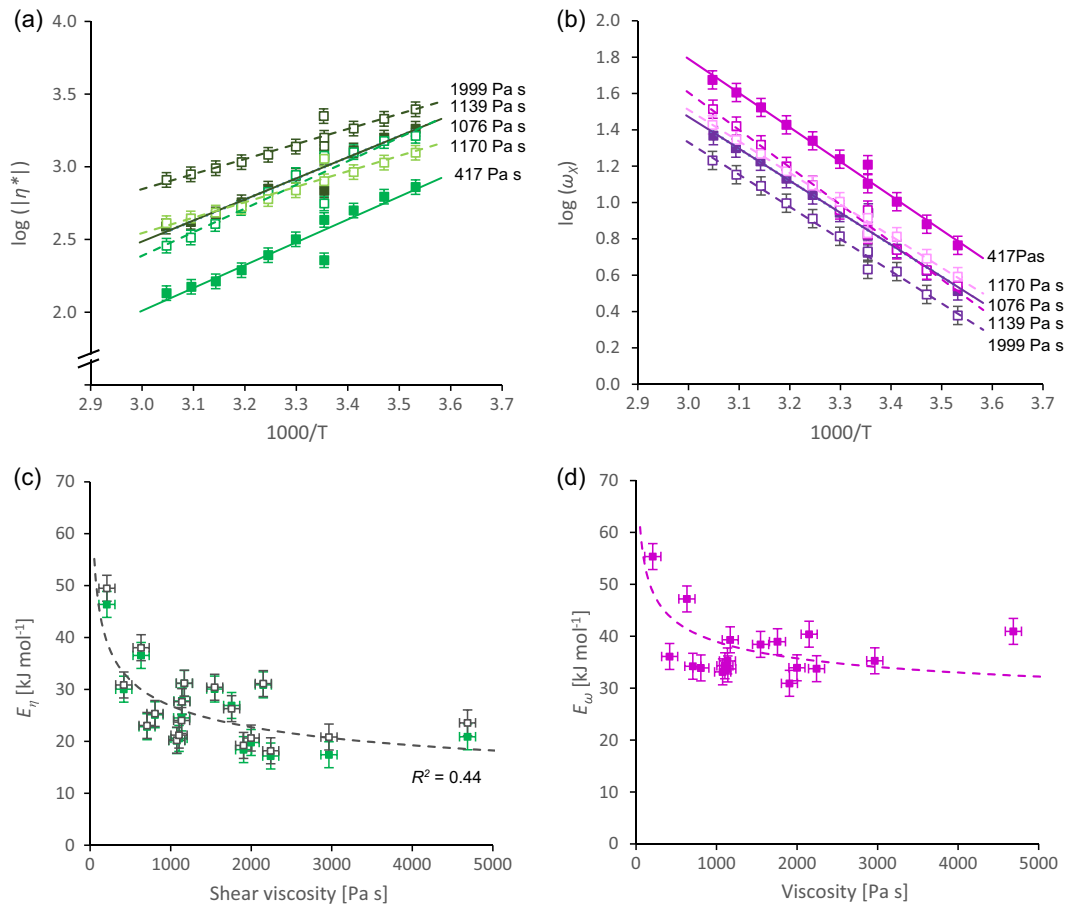


Fig. 5. Temperature dependences in the form of Arrhenius plots, based on (a) modulus of the complex viscosity at 0.63 rad s^{-1} and (b) cross-over frequency. Corresponding values of apparent activation energies derived from (c) calculated zero-shear viscosity (open symbols) and modulus of complex viscosity at 0.63 rad s^{-1} (filled symbols) and (d) cross-over frequency, plotted against shear viscosity at $25 \text{ }^\circ\text{C}$. The dashed line in (c) represents the best fit through the data using Eq. (7); the dashed line in (d) represents the best fit through the data using Eq. (8b). The error bars in (c) and (d) were obtained by manually fitting plausible trend lines with the greatest and least slopes through the Arrhenius plots (as in Fig. 3 or Fig. 5a and b).

$$a_T = \frac{\omega(T)}{\omega(T_0)} \quad (9)$$

A similar expression can also be used for the modulus (vertical) axis.

For an amorphous polymer at temperatures close to its glass transition (T_g), the availability of free volume for segmental motion is believed to limit the dynamic behaviour. Under these conditions, it is expected that the temperature dependence of the TTS scaling parameters would be described by the Williams, Landel and Ferry (WLF) equation [73]:

$$\log(a_T) = \frac{c_1(T - T_0)}{c_2 + T - T_0} \quad (10)$$

The constants c_1 and c_2 are essentially empirical, but are related to the amount of free volume in the system and how it changes with temperature, which is usually characterised by a sudden increase in thermal expansion above T_g [68,69].

The greater availability of free volume in polymer solutions or melts at temperatures much higher than T_g ($T > T_g + 100 \text{ }^\circ\text{C}$) is expected to impose less of a limiting factor. Under these conditions, the flow behaviour often follows an Arrhenius model. In this case, the TTS parameter is described by:

$$\log(a_T) = \frac{kE_a}{2.303R} \left(\frac{1}{T} - \frac{1}{T_0} \right) \quad (11)$$

This appeared to be the case for the silk feedstock specimens investigated here. Whether reflecting a true activation energy or temperature dependence due to other factors, it was found that the horizontal shift factor (a_T) could be obtained using Eq. (11), with the value of E_ω extracted from an Arrhenius plot of cross-over frequency.

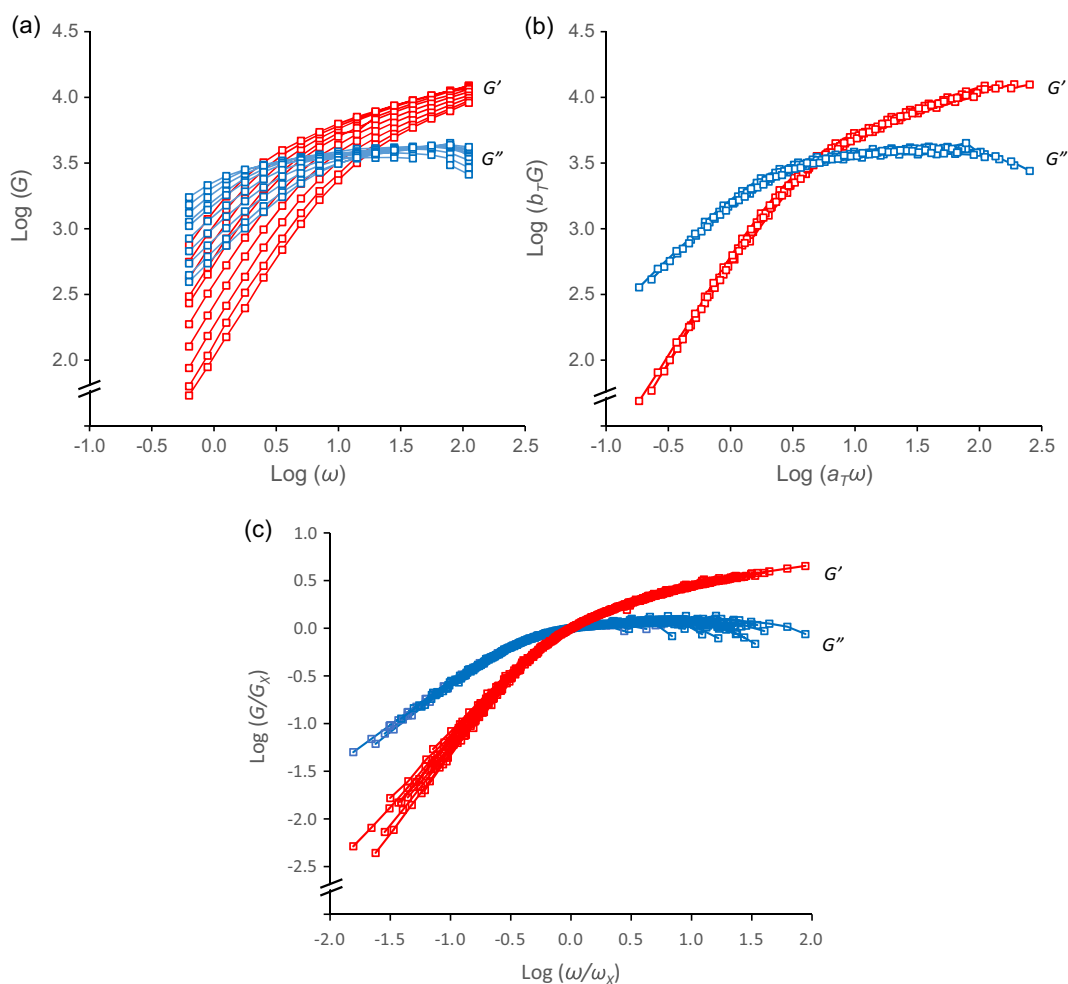


Fig. 6. Time-temperature superposition of oscillatory data for a native silk feedstock specimen with $\eta_1 = 1757$ Pa s at 25 °C: (a) as measured at different temperatures between 10 and 55 °C; (b) after shifting the angular frequency and modulus values to the reference temperature of 25 °C. Note: the frequency shift corresponded to $E_\omega = 39$ kJ mol⁻¹, which agreed with the value extracted from an Arrhenius plot for these data. A vertical shift equivalent to $E_V = 4$ kJ mol⁻¹ was also applied to these data. (c) A combination of TTS and normalisation with respect to the cross-over modulus and frequency, using data measured between 5 and 50 °C for six specimens with $\eta_1 = 418$ –3304 Pa s at 25 °C.

Generally, a small vertical shift factor (b_T) was also required for a successful superposition. This was evaluated empirically, after applying the horizontal shift and was typically equivalent to $E_V < 8$ kJ mol⁻¹.

For the successful TTS shown in Fig. 6, values of $E_\omega = 39$ kJ mol⁻¹ and $E_V = 4$ kJ mol⁻¹ were used. Similarly good transformations were also achieved for the other specimens (with η_1 ranging from 208 to 4686 Pa s at 25 °C), consistent with their rheological behaviour being controlled by an activation energy. This suggests that the native silk protein specimens were all ‘well-behaved’ polymer solutions – notwithstanding the considerable variations in E_ω or viscosity that were observed between specimens.

It should be emphasised that the master-curves obtained in the present work showed the typical characteristics expected for viscoelastic liquids, with $G' > G''$ at higher frequencies and a cross-over to $G' < G''$ at lower frequencies. These findings contrasted the earlier work by Ochi et al. [50], however, which also attempted TTS with silk feedstock specimens measured over temperatures and frequency ranges similar to those used here. Although that work successfully compiled master-curves from the oscillatory data measured between 15 and 55 °C, the results consistently showed $G' > G''$ over the entire frequency range, which suggested that the samples used had already gelled.

One further point merits mention. It was shown previously [37] that oscillatory data measured at 25 °C for *B. mori* silk feedstock specimens with considerably different shear viscosities (706–2242 Pa s) could be compiled onto a master-curve by normalising against the cross-over frequency and modulus. We have now demonstrated that data measured for an individual specimen over a range of temperatures can also be compiled onto a master-curve, by TTS. The question arises: can we combine both effects to generate master-curves for all dynamic modulus data from any specimen and temperature, provided it does not undergo a phase change?

Based on experiments to date, this appeared to be the case, as all oscillatory results generally converged quite well. This is demonstrated in Fig. 6c, based on measurements at 5, 25 and 50 °C from six specimens with $\eta_1 = 418\text{--}3304$ Pa s at 25 °C. Thus, it appeared that the dynamic modulus results for *B. mori* silk feedstocks conformed to a certain shape, although the factors defining the frequency and modulus ranges depended on temperature and could vary between specimens.

It should also be noted that TTS and normalisation against the cross-over do mathematically similar operations. In both cases, the frequency and modulus data are being scaled: however, TTS reflects temperature-dependences inherent in the materials, based on well-established theory, while an explanation for the sample-to-sample variations still eludes us.

4. Discussion

Previous work [37,40] showed that, provided they are handled appropriately (*i.e.* avoiding excessive mechanical stress during excision from the silkworm, peeling off the gland epithelium, loading onto the rheometer and the subsequent measurements), native silk protein feedstocks are well-behaved viscoelastic systems. In the present work, it may be noted that the highest shear stress measured was just below 4.7 kPa (corresponding to the specimen with $\eta_1 = 4685.9$ Pa s at 25 °C), which was below the threshold for stress-induced gelation; hence, the subsequent oscillatory data still showed $G' > G''$ at high frequency and a cross-over to $G'' > G'$ at lower frequencies, typical of a concentrated polymer solution. Moreover, the oscillatory rheology of individual specimens appears to be dominated by two Maxwell-type processes, with relaxation time constants around 0.44 and 0.055 s at 25 °C.

This interpretation is based on the proteins having random coil configurations in the native silk feedstock, despite a considerable body of literature [23,25,26] in which folded structures are proposed. It is useful, therefore, to examine the evidence for and against these apparently contradictory opinions.

Precisely folded tertiary structures are generally expected to play an important part in the biochemical functions of proteins [74,75]. This concept was articulated by Mirsky and Pauling in 1936 [76], although it is related to the earlier 'lock-and-key' hypothesis of enzyme activity proposed by Fischer in 1894 [77]. This provides a very good description of enzyme action in many cases; however, it is clear that this model is not universally applicable to all proteins. In particular, recent work has revealed that many important biochemical functions are performed by intrinsically disordered proteins [38,39]. Compared with 'conventional' globular proteins, IDPs adopt more expanded configurations and exhibit greater conformational dynamics; this may enhance their rates of substrate binding through a 'fly-fishing' mechanism and they may accommodate different binding partners in 'one-to-many' interactions, while more structured chain folding and enzymatic activity may arise in the presence of a substrate.

With respect to the structures of silk proteins, Iizuka [25,26] stated that fibroin 'is obviously in a fairly folded form' in the native silk feedstock solution. Whilst a clear explanation for this statement was not given, it may have been based on the considerable evidence for higher order structures observed in the spun fibres and the leading perspective that all proteins must have folded structures. Nevertheless, in a subsequent paper [28] based on an optical rotatory dispersion study, Iizuka stated that 'the evidence strongly indicates a disordered conformation for silk fibroin in aqueous solution' with 'a lack of any α -helical structure'.

Jin and Kaplan [23] 'suggested the possibility of formation of micellar structures in water'. This was largely based on the arrangement of (so called) hydrophilic and hydrophobic blocks of amino acids identified by sequencing the *B. mori* fibroin gene [78], together with reports by Ochi et al. [50] of fibroin forming polymolecular aggregates in solution. Yet, careful examination of the rheology data presented by Ochi et al. (showing $G' > G''$ across the entire frequency range, in sharp contrast to our own observations) suggested that their specimens had gelled, which may cast doubt on their claims of aggregate formation under normal conditions. Consequently, the experimental evidence for silk proteins forming folded or globular structures in native silk feedstock prior to spinning appears rather tenuous.

In contrast, as discussed previously in this paper and elsewhere [37,72], there is considerable evidence that the silk protein in native feedstock adopts a predominantly random coil conformation (*i.e.* without a specific, folded structure). This has been suggested by CD [28–32] and Raman spectroscopy [24], although both methods require calibration against standards of known conformation. Examination of SANS data reported by Greving et al. [32] revealed a slope of around -2 in a double logarithmic plot of intensity against modulus of the scattering vector, which is consistent with a random coil polymer; moreover, the radius of gyration obtained (around 10 nm) was consistent with a random walk model of a protein containing the expected number of amino acids [78]. Finally, perhaps the most compelling findings are from NMR studies by Asakura and co-workers [33–36]; in addition to chemical shifts consistent with random coil structures in diluted and native silk feedstocks – including material within intact silkworms [35], relaxation times and nuclear Overhauser effects suggested that the fibroin chains exhibited uniform motion typical of polymers in solution.

The work reported here extended our previous studies [37,40], by investigating the flow behaviour over a considerable temperature range. When examined individually, specimens of native silk protein feedstocks exhibited consistent rheological behaviour. Between 2 and 55 °C, the temperature-dependent viscosity or relaxation rates appeared to follow the Arrhenius equation, consistent with the underlying molecular dynamics being controlled by an activation energy. This also argued against any phase changes taking place within the native silk protein specimens under the experimental conditions used, as these would have produced discontinuities or irreversible changes in the flow behaviour, which were not observed.

Previous workers have reported cryoscopically-induced phase changes in *B. mori* silk feedstock specimens on freezing (below 0 °C) [79] and thermally-induced gelation around 68 °C [80]. These temperatures are outside the range used in the present work, which is consistent with phase changes not being observed here. Moreover, although the rheological changes associated with gelation are not explored in the present work, results from our recent investigations into this will be reported separately [72].

Nevertheless, considerable rheological differences were revealed by comparing across the set of specimens analysed. For example: low shear viscosities at 25 °C ranged from 208 to 4686 Pa s, corresponding to cross-over frequencies from 17.7 to 2.1 rad s⁻¹. These observations were consistent with previous findings [37,40] and suggested that the native silk feedstocks were highly variable, in spite of using specimens obtained in a consistent way from the same (middle posterior) division of the silk gland of silkworms at (nominally) the same stage of their lifecycle (5th instar, beginning cocoon construction).

Moreover, the variability between specimens also extended to the temperature dependences of the rheological processes. Apparent activation energies based on viscosity measurements ranged from 17.2 to 49.5 kJ mol⁻¹, showing a weak ($R^2 = 0.44$) inverse correlation with the viscosity. Hence, the specimens with higher viscosities exhibited the lowest apparent activation energies of flow, as demonstrated in Fig. 5c. This argues against dismissing the observed variability as experimental uncertainty, but suggests the possibility of a mechanistic link between these parameters. Slightly higher values (from 30.9 to 55.4 kJ mol⁻¹) were obtained from the corresponding cross-over frequency data, but without any clear relationship to the viscosities of the specimens.

To put these findings in context and enable discussion surrounding potential mechanistic explanations for our observations, differences in activation energy of flow have been reported between synthetic polymer systems. Liao et al. reported a steady decrease in E_a (from 37 to 29 kJ mol⁻¹) for molten poly(hydroxybutyrate-co-hydroxyhexanoate) copolymers with up to 10% molar hexanoate content [65]. This demonstrated the effect of polymer composition, in terms of a decrease in dipolar interactions between monomers as the hexanoate content was increased. Similarly, Osterwinter et al. [66] reported E_a values of 71 and 108 kJ mol⁻¹ respectively, for fully methylated and demethylated poly(glycerol) melts, demonstrating the effect of inter-chain hydrogen bonding. These values of E_a also appeared to be independent of molecular weight, suggesting that the strength of interactions between monomers was considerably more important than chain length over the range studied (from ca. 1 to 100 kDa). Sescousse et al. [81] reported increases in viscosity (e.g. from ca. 0.2–30 Pa s at 70 °C) and activation energy (from ca. 40 to 65 kJ mol⁻¹), as the concentration of cellulose dissolved in imidazolium-based ionic liquids was increased from 0.2 to 16%. Shulyak et al. [82] also reported small increases in viscosity and E_a (from 15.3 to 17.82 kJ mol⁻¹) for dilute aqueous solutions of poly(ethylene glycol) at 25 °C. Conversely, Rwei and Lyu [67] reported increases in viscosity (from ca. 2000–5500 Pa s at 25 °C) accompanied by significant decreases in activation energy (from ca. 60 to 15 kJ mol⁻¹) as the concentration of hydroxypropyl cellulose in aqueous phosphoric acid was increased (from 15 to 38%) and the solution changed from isotropic to liquid crystalline. These authors also demonstrated a dependence on the solvent composition, through increases in activation energy (from 20 to 50 kJ mol⁻¹) with H₃PO₄ content of the binary solvent for isotropic solutions. In each of these examples, it appeared that the activation energy for flow was dominated by the strength of interactions between monomers. This can be interpreted in terms of a segmental friction coefficient, representing the ease with which chain segments can slide past each other during reptation [71]. Hence, the variability in E_a observed between specimens of native silk protein feedstock may indicate significant compositional variations, which could involve the proteins present or the constituents of the solvent.

Several potential explanations for the variability in viscosity were suggested previously [37,40], but appear less plausible in the light of the results presented here. Hence, protein concentration would be expected to exert an effect; however, only a weak positive correlation ($R^2 = 0.21$) was found [40], which could not explain the range of viscosities observed. Moreover, for regular (i.e. not liquid crystalline) solutions, the activation energy would be expected to increase with viscosity (rather than decrease, as observed). The onset of liquid crystallinity also appears unlikely, as this should produce a negative correlation between viscosity and concentration (which was not seen). Secondly, some variation in the molecular weight of the main (fibroin heavy chain) protein has been reported, with a range of around 15% (from ca. 350 to 410 kDa) between the longest and shortest chains [83], probably resulting from differential splicing or recombination errors, due to the highly repetitive nature of the amino-acid sequence [84]. Nevertheless, this variation in protein length also appeared insufficient to explain the range of viscosities observed, where a change in molecular weight in this reported range would not be expected to affect the activation energies.

Therefore, in addition to the variability shown by rheological characteristics, it is necessary to seek explanations for the inverse relationship between the low shear rate viscosity and E_a . It is not clear why the viscosity should show a weak inverse relationship to a true activation energy of flow; however, it might be easier to explain a relationship with other factors affecting the temperature dependence of flow. Hence, for the native silk feedstock specimens, several hypotheses may be predicated on variations in the strength of interactions between protein chains. Weaker interactions may undergo thermal dissociation, leading to lower viscosities and a greater temperature dependence. At the other extreme, stronger interactions that are less prone to thermal dissociation could produce higher viscosities but smaller temperature dependence.

Differences in the strengths of inter-chain interactions could arise in various ways. There might be changes in the proportions of different proteins present within the native silk feedstock specimens. Dong et al. [6] demonstrated that silk from *B. mori* is a complex mixture of at least 500 proteins that varies between developmental stages, although it is not known whether similar changes may happen over shorter timescales during our sample collection (typically hours to a few days), consistent with cocoon construction. The strengths of inter-chain interactions might also be affected by pH or ionic content

of the native silk protein feedstock. Indeed, Terry et al. [44] demonstrated a reversible increase in G' when specimens from *B. mori* were acidified using acetic acid vapour, while Chen et al. [29,45] and Dicko et al. [30] have discussed the potential role of pH and K ions during spider silk spinning. It is also known that proteins can undergo various types of 'post-translational modifications' [85]. In particular, numerous serine phosphorylations have been observed in both spider [86] and *B. mori* silks [87], which may be expected to affect the interactions with the solvent and between protein chains. Aspects of these various hypotheses are presently under investigation and will be reported at a later date.

Finally, one may speculate as to what – if any – advantage controlling the temperature dependence of the silk feedstock viscosity might confer on the silkworm. Using Eq. (11) with the values obtained for E_{η} (17.2–49.5 kJ mol⁻¹) suggested variations in viscosity ranging from 18 to 61%, over the typical range of ambient temperatures experienced by *B. mori* (20–28 °C [57,88]), with greater consistency at higher viscosity. Arguably, flow characteristics that change with temperature are unavoidable features of a polymer solution. Hence, the silkworm may find it easier to extrude the feedstock when the ambient temperature is higher and the viscosity is lower. Conversely, however, higher viscosity may convey a greater sensitivity towards flow-induced gelation, facilitating fibre formation. It may be interesting to speculate whether these rheological factors are important for the spinning behaviour of the animal and its response to environmental changes, in order to produce silk that is fit for its purpose [89].

5. Conclusions

We report that the rheological temperature dependence of native feedstocks from *B. mori* appear to be well-behaved and follow the Arrhenius equation. This was consistent with flow behaviour governed by an (apparent) activation energy and culminated in the ability to transform oscillatory data onto a master-curve, in accordance with the time-temperature superposition principle. Thermally-induced phase changes, which would have produced deviations or irreversible changes in thermal responses, were not observed in the temperature range used (2–55 °C). This contradicted a previous report [47] of native silk protein feedstocks from *B. mori* undergoing irreversible gelation from 35 °C.

At the same time, however, considerable variability was observed between specimens in their temperature dependence, consistent with differences in the (apparent) activation energy of flow between specimens. This implied an underlying physical mechanism linking the parameters, with the influence of pH, ions and post translational modification of the silk proteins being suggested as future areas to explore. It is also not known whether this relationship represents an evolutionary constraint to the silkworm, through some aspect of fibre spinning, or if it was a purely coincidental feature of the native silk protein feedstocks. Yet its presence clearly effects the flow properties of these materials and, thus, warrants further investigation if we are to truly understand how silk is spun.

Acknowledgements

This work was funded by the EPSRC, project reference EP/K005693/1.

References

- [1] C.L. Craig, Evolution of arthropod silks, *Annu. Rev. Entomol.* 42 (1997) 231–267, <http://dx.doi.org/10.1146/annurev.ento.42.1.231>.
- [2] M.A. Collin, J.S. Edgerley, C.Y. Hayashi, Comparison of fibroin cDNAs from webspinning insects: insight into silk formation and function, *Zoology* 114 (2011) 239–246, <http://dx.doi.org/10.1016/j.zool.2011.01.004>.
- [3] T.D. Sutherland, J.H. Young, S. Weisman, C.H. Hayashi, D.J. Merritt, Insect silk: one name, many materials, *Annu. Rev. Entomol.* 55 (2010) 171–188, <http://dx.doi.org/10.1146/annurev-ento-112408-085401>.
- [4] F. Sehnal, T. Sutherland, Silks produced by insect labial glands, *Prion* 2 (2008) 145–153, <http://dx.doi.org/10.4161/pri.2.4.7489>.
- [5] M. Boulet-Audet, F. Vollrath, C. Holland, Identification and classification of silks using infrared spectroscopy, *J. Exp. Biol.* 218 (2015) 3138–3149, <http://dx.doi.org/10.1242/jeb.128306>.
- [6] Z. Dong, P. Zhao, C. Wang, Y. Zhang, J. Chen, X. Wang, Y. Lin, Q. Xia, Comparative proteomics reveal diverse functions and dynamic changes of *Bombyx mori* silk proteins spun from different development stages, *J. Proteome Res.* 12 (2013) 5213–5222, <http://dx.doi.org/10.1021/pr4005772>.
- [7] M.A. Collin, K. Mita, F. Sehnal, C.Y. Hayashi, Molecular evolution of lepidopteran silk proteins: insights from the ghost moth, *Hepialus californicus*, *J. Mol. Evol.* 70 (2010) 519–529, <http://dx.doi.org/10.1007/s00239-010-9349-8>.
- [8] N. Yonemura, F. Sehnal, The design of silk fiber composition in moths has been conserved for more than 150 million years, *J. Mol. Evol.* 63 (2006) 42–53, <http://dx.doi.org/10.1007/s00239-005-0119-y>.
- [9] L. Brunetta, C.L. Craig, *Spider Silk*, Yale University Press, New Haven, 2010.
- [10] L. Eisoldt, A. Smith, T. Scheibel, Decoding the secrets of spider silk, *Mater. Today* 14 (2011) 80–86, [http://dx.doi.org/10.1016/S1369-7021\(11\)70057-8](http://dx.doi.org/10.1016/S1369-7021(11)70057-8).
- [11] F. Vollrath, D.P. Knight, Liquid crystalline spinning of spider silk, *Nature* 410 (2001) 541–548.
- [12] F. Vollrath, B. Madsen, Z. Shao, The effects of spinning conditions on the mechanics of a spider's dragline silk, *Proc. R. Soc. Lond. B* 268 (2001) 2339–2346, <http://dx.doi.org/10.1098/rspb.2001.1590>.
- [13] A.A. Walker, C. Holland, T.D. Sutherland, More than one way to spin a crystallite: multiple trajectories through liquid crystallinity to solid silk, *Proc. Roy. Soc. B* 282 (2015), <http://dx.doi.org/10.1098/rspb.2015.0259>. 2015.0259.
- [14] X. Liu, K-Q. Zhang, Silk Fiber - molecular formation mechanism, structure-property relationship and advanced applications, in: C. Lesieur (Ed.), *Oligomerization of Chemical and Biological Compounds*, InTech, 2014, <http://dx.doi.org/10.5772/57611>.
- [15] A.J. Ryan, A.N. Wilkinson, *Polymer Processing and Structure Development*, Kluwer Academic Publishers, Dordrecht, 1998.
- [16] R.W. Moncrief, *Man-Made Fibres*, Newnes-Butterworths, London, 1975.
- [17] M. Boulet-Audet, A.E. Terry, F. Vollrath, C. Holland, Silk protein aggregation kinetics revealed by Rheo-IR, *Acta Biomater* 10 (2014) 776–784, <http://dx.doi.org/10.1016/j.actbio.2013.10.032>.
- [18] C. Holland, J.S. Urbach, D.L. Blair, Direct visualization of shear dependent silk fibrillogenesis, *Soft Matter* 8 (2012) 2590–2594, <http://dx.doi.org/10.1039/c2sm06886a>.

- [19] C. Holland, F. Vollrath, A.J. Ryan, O.O. Mykhaylyk, Silk and synthetic polymers: reconciling 100 degrees of separation, *Adv. Mater.* 24 (2012) 105–109, <http://dx.doi.org/10.1002/adma.201103664>.
- [20] C. Holland, K. O'Neil, F. Vollrath, C. Dicko, Distinct structural and optical regimes in natural silk spinning, *Biopolymers* 97 (2012) 368–373, <http://dx.doi.org/10.1002/bip.22022>.
- [21] C. Fu, Z. Shao, F. Vollrath, Animal silks: their structures, properties and artificial production, *Chem. Commun.* (2009) 6515–6529, <http://dx.doi.org/10.1039/b911049f>.
- [22] D.P. Knight, M.M. Knight, F. Vollrath, Beta transition and stress-induced phase separation in the spinning of spider dragline silk, *Int. J. Biol. Macromol.* 27 (2000) 205–210, [http://dx.doi.org/10.1016/S0141-8130\(00\)00124-0](http://dx.doi.org/10.1016/S0141-8130(00)00124-0).
- [23] H.-J. Jin, D.L. Kaplan, Mechanism of silk processing in insects and spiders, *Nature* 424 (2003) 1057–1061.
- [24] J. Magoshi, Y. Magoshi, S. Nakamura, Physical properties and structure of silk: 10. The mechanism of fibre formation from liquid silk of silkworm *Bombyx mori*, *Polym. Commun.* 26 (1985) 309–311.
- [25] E. Iizuka, Silk thread: mechanism of spinning and its mechanical properties, *J. Appl. Polym. Sci. Appl. Polym. Sympos.* 41 (1985) 173–185.
- [26] E. Iizuka, Mechanism of fibre formation by the silkworm *Bombyx mori* L., *Biorheology* 3 (1966) 141–152.
- [27] C. Foà, The colloidal characteristics of natural silk, *Kolloid Z.* 10 (1912) 7–12.
- [28] E. Iizuka, J.T. Yang, The disordered and β conformations of silk fibroin in solution, *Biochemistry* 7 (1968) 2218–2228.
- [29] X. Chen, Z. Shao, F. Vollrath, The spinning processes for spider silk, *Soft Matter* 2 (2006) 448–451, <http://dx.doi.org/10.1039/b601286h>.
- [30] C. Dicko, J.M. Kenney, D. Knight, F. Vollrath, Transition to a β -sheet-rich structure in spidroin in vitro: the effects of pH and cations, *Biochemistry* 43 (2004) 14080–14087, <http://dx.doi.org/10.1021/bi0483413>.
- [31] C. Dicko, D. Knight, J.M. Kenney, F. Vollrath, Structural conformation of spidroin in solution: a synchrotron radiation circular dichroism study, *Biomacromolecules* 5 (2004) 758–767, <http://dx.doi.org/10.1021/bm034373e>.
- [32] I. Greving, C. Dicko, A. Terry, P. Callow, F. Vollrath, Small angle neutron scattering of native and reconstituted silk fibroin, *Soft Matter* 6 (2010) 4389–4395, <http://dx.doi.org/10.1039/c0sm00108b>.
- [33] T. Asakura, K. Okushita, M.P. Williamson, Analysis of the structure of *Bombyx mori* silk fibroin by NMR, *Macromolecules* 48 (2015) 2345–2357, <http://dx.doi.org/10.1021/acs.macromol.5b00160>.
- [34] C. Zhao, T. Asakura, Structure of silk studied with NMR, *Prog. Nucl. Mag. Res. Spectrosc.* 39 (2001) 301–352.
- [35] T. Asakura, Y. Watanabe, A. Uchida, A.H. Minagawa, NMR of silk fibroin. 2. ^{13}C NMR study of the chain dynamics and solution structure of *Bombyx mori* silk fibroin, *Macromolecules* 17 (1984) 1075–1081.
- [36] T. Asakura, H. Suzuki, Y. Watanabe, Conformational characterization of silk fibroin in intact *Bombyx mori* and *Philosamia cynthia ricini* silkworms by ^{13}C NMR spectroscopy, *Macromolecules* 16 (1983) 1024–1026.
- [37] P.R. Laity, C. Holland, Native silk feedstock as a model biopolymer: a rheological perspective, *Biomacromolecules* 17 (2016) 2662–2671, <http://dx.doi.org/10.1021/acs.biomac.6b00709>.
- [38] P. Tompa, Intrinsically disordered proteins: a 10-year recap, *Trends Biochem. Sci.* 37 (2012) 509–516, <http://dx.doi.org/10.1016/j.tibs.2012.08.004>.
- [39] V.N. Uversky, Intrinsically disordered proteins and their environment: effects of strong denaturants, temperature, pH, counter ions, membranes, binding partners, osmolytes, and macromolecular crowding, *Protein J.* 28 (2009) 305–325, <http://dx.doi.org/10.1007/s10930-009-9201-4>.
- [40] P.R. Laity, S.E. Gilks, C. Holland, Rheological behaviour of native silk feedstocks, *Polymer* 67 (2015) 28–39, <http://dx.doi.org/10.1016/j.polymer.2015.04.049>.
- [41] C. Holland, D. Porter, F. Vollrath, Comparing the rheology of mulberry and 'wild' silkworm spinning dopes, *Biopolymers* 97 (2012) 362–367, <http://dx.doi.org/10.1002/bip.22011>.
- [42] C. Holland, A.E. Terry, D. Porter, F. Vollrath, Natural and unnatural silks, *Polymer* 48 (2007) 3388–3392, <http://dx.doi.org/10.1016/j.polymer.2007.04.019>.
- [43] C. Holland, A.E. Terry, D. Porter, F. Vollrath, Comparing the rheology of native spider and silkworm spinning dope, *Nature Mater.* (2006) 870–874, <http://dx.doi.org/10.1038/nmat1762>.
- [44] A.E. Terry, D.P. Knight, D. Porter, F. Vollrath, PH induced changes in the rheology of silk fibroin solution from the middle division of *Bombyx mori* silkworm, *Biomacromolecules* 5 (2004) 768–772, <http://dx.doi.org/10.1021/bm034381v>.
- [45] X. Chen, D.P. Knight, F. Vollrath, Rheological characterization of *Nephila* spidroin solution, *Biomacromolecules* 3 (2002) 644–648, <http://dx.doi.org/10.1021/bm0156126>.
- [46] Y. Jin, Y. Hang, J. Juo, Y. Zhang, H. Shao, X. Hu, *In vitro* studies on the structure and properties of silk fibroin aqueous solutions in silkworm, *Int. J. Biol. Macromol.* 62 (2013) 162–166, <http://dx.doi.org/10.1016/j.ijbiomac.2013.08.027>.
- [47] M. Moriya, F. Roschztardt, Y. Nakahara, H. Saito, Y. Masabuchi, T. Asakura, Rheological properties of native silk fibroins from domestic and wild silkworms, and flow analysis in each spinneret by a finite element method, *Biomacromolecules* 10 (2009) 929–935, <http://dx.doi.org/10.1021/bm801442g>.
- [48] M. Moriya, K. Ohgo, Y. Masubuchi, T. Asakura, Flow analysis of aqueous solution of silk fibroin in the spinneret of *Bombyx mori* silkworm by combination of viscosity measurement and finite element method calculation, *Polymer* 49 (2008) 952–956, <http://dx.doi.org/10.1016/j.polymer.2007.12.032>.
- [49] H. Wang, N. Mao, X. Hu, H. Shao, X. Jin, The properties of native silk fibroin (SF) solution/gel from *Bombyx mori* silkworms during the full fifth instar larval stage, *J. Wuhan Univ. Technol.-Mater. Sci. Ed.* 26 (2011) 262–268, <http://dx.doi.org/10.1007/s11595-011-0210-8>.
- [50] A. Ochi, K.S. Hossain, J. Magoshi, N. Nemoto, Rheology and dynamic light scattering of silk fibroin solution extracted from the middle division of *Bombyx mori* silkworm, *Biomacromolecules* 3 (2002) 1187–1196, <http://dx.doi.org/10.1021/bm020056g>.
- [51] N. Kojić, J. Bico, C. Clasen, G.H. McKinley, *Ex vivo* rheology of spider silk, *J. Exp. Biol.* 209 (2006) 4355–4362, <http://dx.doi.org/10.1242/jeb.02516>.
- [52] O. Kukal, Winter mortality and the function of larval hibernacula during the 14-year life cycle of an arctic moth, *Gynaephora groenlandica*, *Can. J. Zool.* 73 (1995) 657–662, <http://dx.doi.org/10.1139/z95-077>.
- [53] V. Mhuka, S. Dube, M.M. Nindi, Chemical, structural and thermal properties of *Gonometa postica* silk fibroin, a potential biomaterial, *Int. J. Biol. Macromol.* 52 (2013) 305–311, <http://dx.doi.org/10.1139/z95-077>.
- [54] T. Krakauer, Thermal responses of the orb-weaving spider, *Nephila clavipes* (Araneae: Argiopidae), *Am. Midl. Nat.* 88 (1972) 245–250.
- [55] Y.-C. Su, Y.-H. Chang, S.-C. Lee, I.-M. Tso, Phylogeography of the giant wood spider (*Nephila pilipes*, Araneae) from Asian-Australian regions, *J. Biogeogr.* 34 (2007) 177–191, <http://dx.doi.org/10.1111/j.1365-2699.2006.01617.x>.
- [56] J.R. Henschel, Diet and foraging behaviour of huntsman spiders in the Namib dunes (Araneae: Heteropodidae), *J. Zool. Lond.* 234 (1994) 239–251.
- [57] L.E. Barghusen, D.L. Claussen, M.S. Anderson, A.J. Bailer, The effects of temperature on the web-building behaviour of the common house spider, *Achaearanea tepidariorum*, *Funct. Ecol.* 11 (1997) 4–10, <http://dx.doi.org/10.1046/j.1365-2435.1997.00040.x>.
- [58] F. Vollrath, B. Madsen, Z. Shao, The effect of spinning conditions on the mechanics of a spider's dragline silk, *Proc. R. Soc. Lond. B.* 268 (2001) 2339–2346, <http://dx.doi.org/10.1098/rspb.2001.1590>.
- [59] F. Vollrath, M. Downes, S. Krackow, Design variability in web geometry of an orb-weaving spider, *Physiol. Behav.* 62 (1997) 735–743, [http://dx.doi.org/10.1016/S0031-9384\(97\)00186-8](http://dx.doi.org/10.1016/S0031-9384(97)00186-8).
- [60] Y.L. Ramachandra, G. Bali, S.P. Rai, Effect of temperature and relative humidity on spinning behaviour of silkworm (*Bombyx mori* L.), *Indian J Exp Biol* 39 (2001) 87–89.
- [61] J. Dealy, D. Plazek, Time-temperature superposition – a user's guide, *Rheol. Bull.* 78 (2009) 16–31.
- [62] R.G. Larson, *The Structure and Rheology of Complex Fluids*, Oxford University Press, 1999.
- [63] R.I. Tanner, *Engineering Rheology*, Clarendon Press, Oxford, 1985.
- [64] J.D. Ferry, *Viscoelastic Properties of Polymers*, third ed., John Wiley & Sons Inc, 1980.

- [65] Q. Liao, I. Noda, C.W. Frank, Melt viscoelasticity of biodegradable poly(hydroxybutyrate-co-3-hydroxyhexanoate) copolymers, *Polymer* 50 (2009) 6139–6148, <http://dx.doi.org/10.1016/j.polymer.2009.10.049>.
- [66] C. Osterwinter, C. Schubert, C. Tonhauser, D. Wilms, H. Frey, C. Friedrich, Rheological consequences of hydrogen bonding: linear viscoelastic response of linear polyglycerol and its permethylated analogues as a general model for hydroxyl-functional polymers, *Macromolecules* 48 (2015) 119–130, <http://dx.doi.org/10.1016/j.polymer.2009.10.049>.
- [67] S.-P. Rwei, M.-S. Lyu, HPC/H₂O/H₃PO₄ tertiary system: a rheological study, *Cellulose* 20 (2013) 135–147, <http://dx.doi.org/10.1007/s10570-012-9810-5>.
- [68] I.M. Ward, D.W. Hadley, *An Introduction to the Mechanical Properties of Solid Polymers*, John Wiley & Sons Ltd., Chichester, UK, 1993.
- [69] J.M.G. Cowie, *Polymers: Chemistry and Physics of Modern Materials*, second edn., Chapman & Hall, London, 1991.
- [70] J.W. Goodwin, R.W. Hughes, *Rheology for Chemists*, Royal Society of Chemistry, Cambridge, 2008.
- [71] M. Doi, S.F. Edwards, *The Theory of Polymer Dynamics*, Clarendon Press, Oxford, 1986.
- [72] P.R. Laity, C. Holland, The rheology behind stress-induced solidification in native silk feedstocks, *Int. J. Mol. Sci.* 17 (2016) 1812, <http://dx.doi.org/10.3390/ijms17111812>.
- [73] M.L. Williams, R.F. Landel, J.D. Ferry, The temperature dependence of relaxation mechanisms in amorphous polymers and other glass-forming liquids, *J. Am. Chem. Soc.* 77 (1955) 3701–3707.
- [74] D. Whitford, *Proteins Structure and Function*, John Wiley and Sons Ltd., Chichester, UK, 2005.
- [75] A. Fersht, *Structure and Mechanism in Protein Science: A Guide to Enzyme Catalysis and Protein Folding*, W.H. Freeman and Co., New York, 1999.
- [76] A.E. Mirsky, L. Pauling, On the structure of native, denatured and coagulated proteins, *Proc. Nat. Acad. Sci.* 22 (1936) 439–447.
- [77] E. Fischer, Einfluss der Configuration auf die Wirkung der Enzyme (Influence of conformation on the effect of enzymes), *Ber. Deut. Chem. Ges.* 27 (1894) 2985–2993.
- [78] C.-Z. Zhou, F. Confalonieri, N. Medina, Y. Zivanovic, C. Esnault, T. Yang, M. Jacquet, J. Janin, M. Duguet, R. Perasso, Z.-G. Li, Fine organization of *Bombyx mori* fibroin heavy chain gene, *Nucl. Acids Res.* 28 (2000) 2413–2419.
- [79] W. Ramsden, Coagulation by shearing and freezing, *Nature* 142 (1938) 1120–1121.
- [80] T. Tanaka, J. Magoshi, Y. Magoshi, S. Inoue, M. Kobayashi, H. Tsuda, M.A. Becker, S. Nakamura, Thermal properties of *Bombyx mori* and several wild silkworm silks, phase transition of liquid silk, *J. Therm. Anal. Calorim.* 70 (2002) 825–832.
- [81] R. Sescousse, K.A. Le, M.E. Ries, T. Budtova, Viscosity of cellulose-imidazolium-based ionic liquid solutions, *J. Phys. Chem. B* 114 (2010) 7222–7228, <http://dx.doi.org/10.1021/jp1024203>.
- [82] I.V. Shulyak, E.I. Grushova, A.M. Semenchenko, Rheological properties of aqueous solutions of polyethylene glycols with various molecular weights, *Rus. J. Phys. Chem. A* 85 (2011) 419–422, <http://dx.doi.org/10.1134/S0036024411030265>.
- [83] R.F. Manning, L.P. Gage, Internal structure of the silk fibroin gene of *Bombyx mori*. II Remarkable polymorphism of the organization of crystalline and amorphous coding sequences, *J. Biol. Chem.* 255 (1980) 9451–9457.
- [84] C.L. Craig, C. Riekel, Comparative architecture of silks, fibrous proteins and their encoding genes in insects and spiders, *Comp. Biochem. Physiol. B* 133 (2002) 493–507, [http://dx.doi.org/10.1016/S1096-4959\(02\)00095-7](http://dx.doi.org/10.1016/S1096-4959(02)00095-7).
- [85] M. Mann, O.N. Jensen, Proteomic analysis of post-translational modifications, *Nature Biotechnol.* 21 (2003) 255–261, <http://dx.doi.org/10.1038/nbt0303-255>.
- [86] J.R. Aparecido dos Santos-Pinto, G. Lamprecht, W.-Q. Chen, S. Heo, J.G. Hardy, H. Priewalder, T.R. Scheibel, M.S. Palma, G. Lubec, Structure and post-translational modifications of the web silk protein spidroin-1 from *Nephila* spiders, *J. Proteom.* 105 (2014) 174–185, <http://dx.doi.org/10.1016/j.jprot.2014.01.002>.
- [87] W.-Q. Chen, H. Priewalder, J.P. Pradeep, G. Lubec, Silk cocoon of *Bombyx mori*: proteins and posttranslational modifications – heavy phosphorylation and evidence for lysine-mediated cross links, *Proteomics* 10 (2010) 369–379, <http://dx.doi.org/10.1002/pmic.200900624>.
- [88] V.K. Rahmathulla, Management of climatic factors for successful silkworm (*Bombyx mori* L.) crop and higher silk production: a review, *Psyche* (2012) 121234, <http://dx.doi.org/10.1155/2012/121234>.
- [89] C. Offord, F. Vollrath, C. Holland, Environmental effects on the construction and physical properties of *Bombyx mori* cocoons, *J. Mater. Sci.* 51 (2016) 10863–10872, <http://dx.doi.org/10.1007/s10853-016-0298-5>.